Advanced Structured Materials

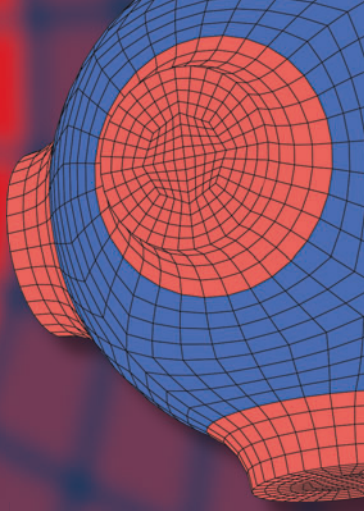

Andreas Öchsner
Holm Altenbach *Editors*

Improved Performance of Materials

Design and Experimental Approaches

Springer

Advanced Structured Materials

Volume 72

More information about this series at http://www.springer.com/series/8611

Andreas Öchsner · Holm Altenbach
Editors

Improved Performance of Materials

Design and Experimental Approaches

Springer

Editors
Andreas Öchsner
Griffith School of Engineering
Griffith University (Gold Coast Campus)
Southport, QLD
Australia

Holm Altenbach
Faculty of Mechanical Engineering,
Institut für Mechanik
Otto-von-Guericke-University Magdeburg
Magdeburg
Germany

ISSN 1869-8433 ISSN 1869-8441 (electronic)
Advanced Structured Materials
ISBN 978-3-319-59589-4 ISBN 978-3-319-59590-0 (eBook)
DOI 10.1007/978-3-319-59590-0

Library of Congress Control Number: 2017940822

Printed on acid-free paper

This Springer imprint is published by Springer Nature
The registered company is Springer International Publishing AG
The registered company address is: Gewerbestrasse 11, 6330 Cham, Switzerland

Preface

There is a permanent demand to improve the properties and performance of engineering materials and structures. Competitiveness due to cost efficiency (e.g. lighter structures and the corresponding fuel savings for transportation systems) or sustainability (e.g. recyclability or reusability) are nowadays the driving factors for engineering developments. The outcomes of these efforts are difficult to be accurately monitored due to the ongoing evaluation cycles. Thus, this monograph aims at presenting a snapshot of recent developments. The properties covered are related to classical fields of mechanical, thermal, electrical and optical properties as well as related to surface-specific quantities (e.g. roughness, wear and modifications due to surface coatings). The material types which are collected in this monograph range from classical metals, over synthetic materials to composites.

We would like to express our sincere appreciation to the representatives of Springer, in particular to Dr. Christoph Baumann, Senior Editor Engineering, who made this volume possible.

Southport, Australia — Prof. Dr.-Ing. Andreas Öchsner D.Sc.
Magdeburg, Germany — Prof. Dr.-Ing. habil. Dr. h. c. mult. Holm Altenbach

Contents

Optimization on Wear Performance of Anti Wear Additive Added Biolubricant

M.H. Sakinah, M.A. Hassan, K. Kadirgama, Ganesan Kadirgama, D. Ramasamy, A.K. Amirruddin, M.M. Rahman and M.M. Noor

Abstract Waste cooking oil is hard to dispose of and harmful to the environment. Recently, a considerable amount of research has been done to improve the properties of engine oil. In this study, engine oil was blended with waste cooking oil and an oil treatment solution. The blended oil was tested in a tribological wear tester. There are three parameters (rotational speed, loads and ratio of waste cooking oil) was consider in the experiments. Tribology wear and properties of the blended oil were investigated in FESEM. It was found that abrasive wear, adhesive wear, fatigue wear and corrosive wear were introduced during the course of the experiments. Normally, corrosive wear was found to be the main dominant in the tribology wear. It was discovered that 5% addition of waste oil to the engine oil treatment and base lubricant performed better than other oil blends.

Keywords Lubricant · Speeds · Engine · Waste

M.H. Sakinah · M.A. Hassan · K. Kadirgama (✉) · G. Kadirgama · D. Ramasamy
A.K. Amirruddin · M.M. Rahman · M.M. Noor
Faculty of Mechanical Engineering, Universiti Malaysia Pahang, 26600 Pekan, Pahang, Malaysia
e-mail: kumaran@ump.edu.my

M.H. Sakinah
e-mail: sakinah.hisham0704@gmail.com

G. Kadirgama
e-mail: knight_35@hotmail.com

D. Ramasamy
e-mail: Deva@ump.edu.my

A.K. Amirruddin
e-mail: Amirruddin@ump.edu.my

M.M. Rahman
e-mail: Mustafizur@ump.edu.my

M.M. Noor
e-mail: Muhamad@ump.edu.my

A. Öchsner and H. Altenbach (eds.), *Improved Performance of Materials*,
Advanced Structured Materials 72, DOI 10.1007/978-3-319-59590-0_1

1 Introduction

Lubricants are widely used in all fields of manufacturing and industrial applications and commonly used to reduce overheating and friction in a variety of engines, machinery, turbines, and gearboxes. They can also aid in maintaining reliable machine functions, expedite operations and the smooth operations and reduce the risks of failure. Furthermore, lubricants can reduce wear and heat loss from the contact of surfaces in motion, prevent rust, reduce oxidation on the contact surfaces and to act as a seal against dirt, dust and water [1]. Due to that, Therefore, petroleum was initially used as the main base stock lubricant, due to its low cost and superior performance. Unfortunately, the rising price of crude oil all over the world, the environmental awareness from various sectors and the depletion of the crude oil spurred scientists to start developing an alternative fuel and lubricant product from natural resources and agricultural feedstock aiming to replace the fossil products [2]. From the reported works, alternative forms of oil should increase to a volume about 36 billion gallons in 2022 [3]. From 2010 until now, several biolubricants are under investigation in different countries [4], e.g., soybean oils (The USA and South America), rapeseed oil (Europe), Jatropha oil [5, 6] and palm oil, (Asia), [7–10]. Most of the works show results regarding their properties. It was noted that vegetable oil-based bio-lubricants exhibit a high results on their properties and it was perceived that using vegetable oil-based bio-lubricants exhibits high lubricity, a high viscosity index (VI), high flash point and low evaporative losses. Moreover, researchers have reported that biolubricants provide better lubricity than petroleum-based oils [11]. Waste cooking oil can be considered the most promising bio-oil feedstock. As reported by many researchers, bio-fuels produced from waste cooking oils have numerous advantages such as low pollution (CO_2, CO and NOx), low cost and acceptable brake specific fuel consumption. Interest has drawn towards the potential of using waste cooking oil as a lubricant. Kalam [12] experimentally investigated the friction and wear characteristics of a normal lubricant, that is, an additive added lubricant and waste vegetable oil (WVO)-contaminated lubricants. The WVO-contaminated lubricants with amine phosphate as antiwear additive reduced the wear and friction coefficient and increased viscosity. Thus, waste palm oil with a normal lubricant and amine phosphate additive could be used as a lubricant substitute (maximum 4%). Based on four ball tribo testing results, the WVO contaminated lubricant with the presence of antiwear additives shows promising result to do better thermal and oxidative properties of waste vegetable oil consisting long chain saturated fatty acids [13]. Tribological behaviour measurements/factors such as the coefficient of friction (COF), specific wear rate and wear mechanism, play an important role in identifying the tribological performance of the bio-lubricant. In an internal combustion engine, mechanical friction occurs between engine components in contact with each other leading to wear and significant loss of efficiency. Loss of energy due to friction between the piston ring and cylinder liner constitutes 20–40% of total mechanical loss and is regarded as the greatest mechanical friction loss [14]. Different engine lubrication

regimes significantly affect the tribological performance of the engine [15]. Wear occurs on all sliding surfaces. Since wear is a chaotic process, wear studies are mostly hence wear studies are mostly done experimentally due to the limited ability to accurately to simulate wear [16]. There are several mechanisms of wear which include seizure, melting, oxidation, adhesion, abrasion, delamination, fatigue, fretting, corrosion, and erosion [17]. A better lubricant which has great properties can reduce the amount of wear loss. The main objective of this study is to modify the current engine oil properties with waste cooking oil to reduce wear.

2 Experimental Setup

The base oil that was used in this experiment is SAE 40. The oil was obtained from the hostel cafeteria. For the preparation of waste cooking oil as bio-lubricant, waste cooking oil undergoes three different processes: coarse filtering, dewatering, and fine filtering. Figure 1 shows the schematic diagram for the filtration of waste cooking oil. Three samples were explicitly prepared, namely, Sample A which is SAE 40 as a reference lubricant (0% volume composition of waste oil), Sample B which are composed of 95% SAE 40+ 5% waste oil added with 0.3% oil treatment (EOT), Sample C, which is composed of 90% SAE 40+ 10% waste oil added with 0.3% (EOT) oil treatment.

The wear test was conducted under the lubricated sliding condition in compliance with ASTM G133-05 standard. The wear testing involves making linear

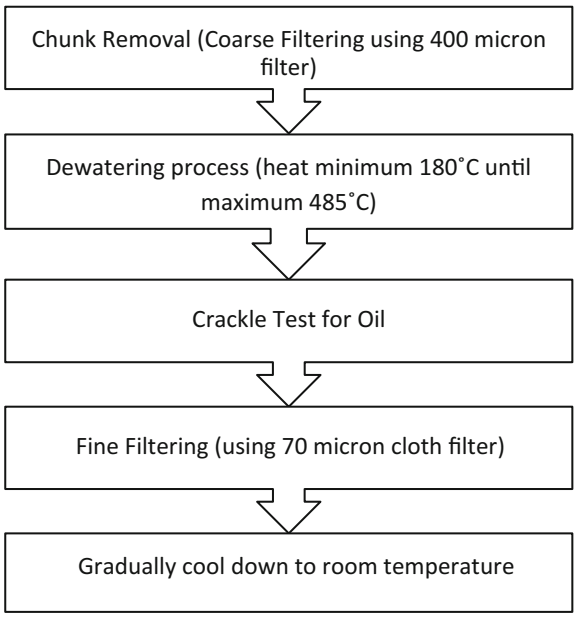

Fig. 1 Schematic diagram for filtration of waste cooking oil

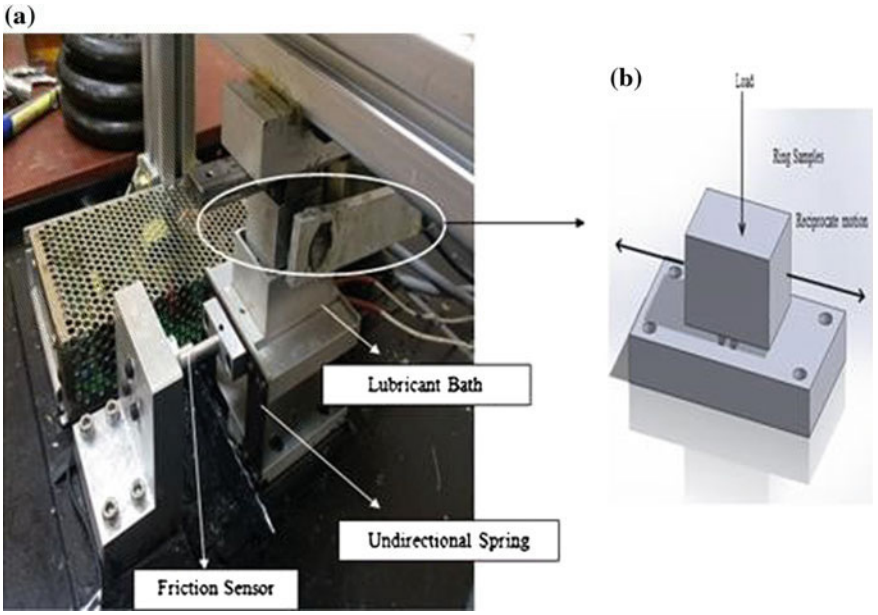

Fig. 2 Experimental setup

movements similar to a cylinder-piston pair operating under real conditions. Figure 2 depicts the wear tester. Normal loads applied to the device by hanging weights on the bearing lever where the piston ring sample is attached in order to produce the desired load. The test will be conducted at engine speed at 200–300 RPM with normal loads 2–9 kg. The temperature that will be used is room temperature and the operating time is 10 min per specimen. The coefficient of Friction (COF) was measured using ARDUINO and the wear rate was determined via weight differences using a weighing scale with a sensitivity of 0.1 mg. The test conditions are presented in Table 1.

The type of material for specimen used in this experiment is Aluminium 6061-T6 which is the material that commonly used for the piston. Flatbar Aluminium 6061-T6 was cut using a band saw and each specimen was prepared 45.12 mm long, 25.14 mm wide and 6 mm thickness. The block was drilled to each side of the rectangle using 4 and 6 mm drill bit. The chemical and physical properties for Aluminium 6061-T6 are shown in the Tables 2 and 3 [18, 19].

Table 1 Tribology test condition

Test specifications	Values
Load, kg	2.0–9.0
Engine Speed, rpm	200–300
Temperature	Room temperature
Operating time	10 min per specimen

Table 2 Chemical composition for Aluminium 6061-T6

Sample	Al	Cr	Cu	Fe	Mg	Mn	Si	Ti	Zn
Percentage (wt%)	95.8	0.04	0.15	0.7	0.8	0.15	0.4	0.14	0.25

Table 3 Physical properties of Aluminium 6061-T6

Properties	Value
Density (g/cc)	2.7
Thermal conductivity (W/m-K)	167
Modulus of elasticity (GPa)	68.9
Specific heat capacity (J/g.°C)	0.896
Melting point (°C)	652

3 Result and Discussion

3.1 Physico-Chemical Properties of Waste Cooking Oil in Base Lubricant

The data were used to evaluate the differences between base lubricant stock (SAE 40) and to serve as a basis for comparing the blended lubricant of palm oil and waste oil. Table 4 shows the properties of base oil (SAE 40), palm oil and waste oil. A good lubricant should have a high boiling point, adequate viscosity, low freezing point, high oxidation resistance, non-corrosive properties and good thermal stability. The most important property of oil is viscosity. It indicates resistance to flow and is directly related to temperature, pressure, and film formation. High viscosity initiates low resistance to flow [1]. Lubricants generally are less dense than water. If the density of an object is less than that of water, then that object will float. This is why if there is a moisture problem in the lubrication system that the water settles to the bottom of the sump and is drained out first whenever the plug is pulled or the valve is opened. The density of a lubricant fluid can provide indications of its composition and nature [20]. Less moisture content in lubricating oil also indicates rust and corrosion prevention.

Table 4 Properties of oil and blended oil

Properties	SAE 40	Waste oil	5% waste oil + SAE 40+ 0.3% EOT	10% waste oil + SAE 40+ 0.3% EOT
Viscosity (mpa.s)	179.2	180.6	176.0	163.2
Density (g/cm^3)	0.8609	0.9049	0.8624	0.8644
Moisture content (%)	0.19	0.28	0.14	0.19

3.2 *Microstructure and Wear Mechanism*

There are various types of wear in a mechanical systems such as abrasive wear, adhesive wear, fatigue wear and corrosive wear. Since the lubricant regime occurred in this experiment was boundary lubrication, therefore, abrasive wear, adhesive wear, fatigue wear and corrosive wear were observed in the wear regions [7]. There were many deep furrows and some corroded areas can be easily seen on surface lubricated with lubricant sample C as shown in Fig. 3a whereas the surface lubricated with lubricant sample A and lubricant sample B are relatively smooth although mark with wear debris due to the rough surface layer on the hard surface from the liner samples touched the soft surface for the piston samples and had close relationships with the thickness of lubricant film as shown in. According to earlier studies, corrosive wear is the main wear mechanism [21] for biolubricant and since the moisture content in the waste oil high which is 0.28% it does give the corrosion effect on the specimen. In sample C it was also observed that the surface of the pins was damaged due to adhesion [22], eventually leading to scuffing and tribo-chemical reactions of sliding contact surfaces as shown in Fig. 3b.

FESEM images of the aluminium plate were obtained using various types of volume concentrations of waste cooking oil blended with engine oil. Referring to Fig. 4, it was found that the honing lines decrease at 5% concentration compare with SAE 40 and wear start to increase when using 10% waste oil concentration [21]. This is due to 5% concentration of waste oil shows the highest viscosity results when compared to 10% concentration because high viscosity (thick) engine oils help to maintain a barrier between moving part and also drag in the movements between two contact surfaces. 10% also show the corroded area on the specimen [19]. According to EDX analysis as in Fig. 4, all specimens have a low percentage of oxygen in the surface of the specimen.

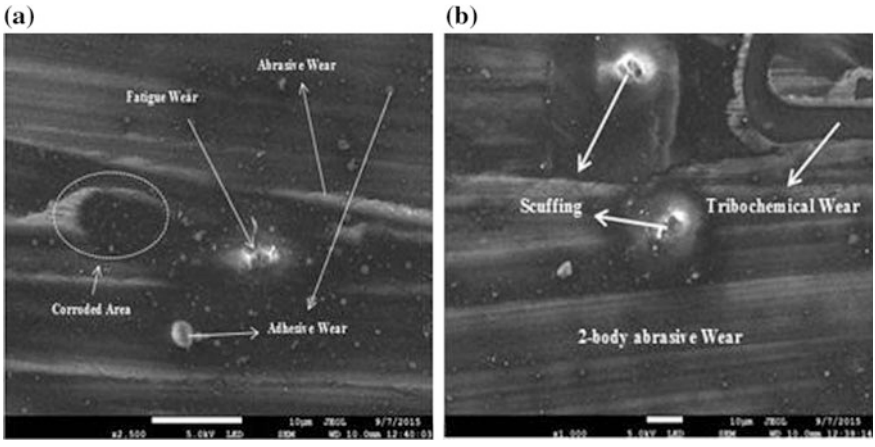

Fig. 3 **a** Sample C with 2500X magnification; **b** Sample C with 1000X magnification

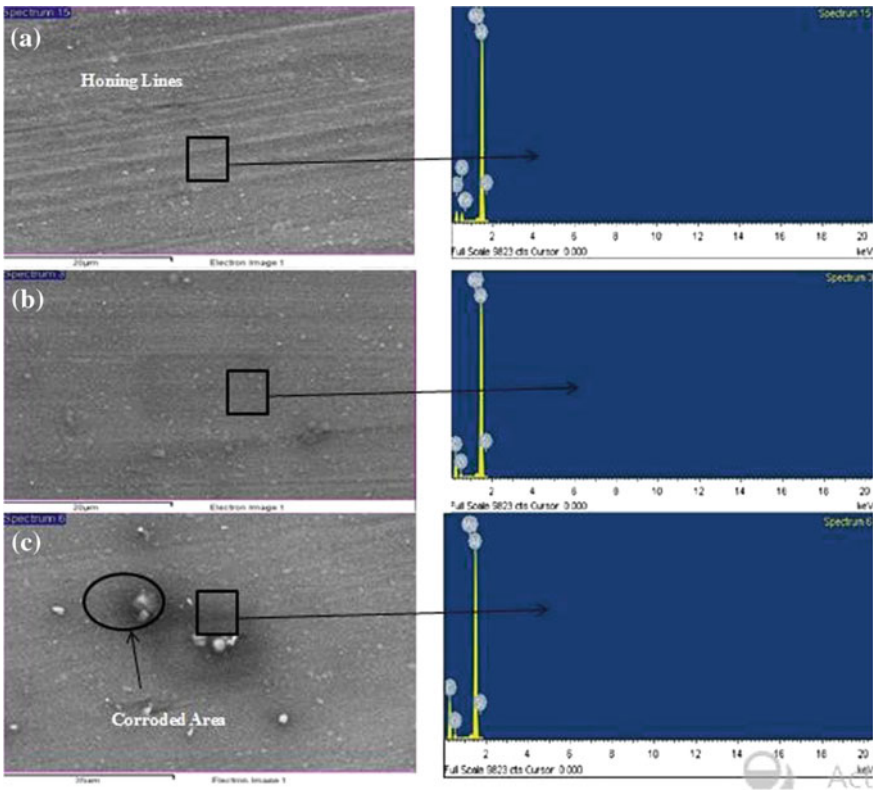

Fig. 4 **a** Sample A; **b** Sample B; Sample C

That means the oxidation occurs during the sliding process due to the water content in the waste palm oil.

4 Conclusion

Based on the experimental study,

(a) According to SEM analysis on the worn surfaces, the maximum wear occurs on at 10% waste oil concentration, while minimum wear occurs at 5% waste oil concentration. concentration of waste oil while minimum wear occurs in 5% concentration waste oil. This shows that waste cooking oil has anti-wear characteristics when small amounts of waste cooking oil are present, and means that using waste cooking oil as an additive for engine oils will not have any severe wear causing consequences, which could potentially lead to premature failure.

(b) In terms of their physico-chemical properties, 5% waste oil added with engine oil treatment were almost identical with the base lubricant.
(c) Engine lubricants formulated from waste oils are renewable, eco-friendly and biodegradable. However, the challenge is an improvement of their performance specifically, with reference to their oxidative stability.

References

1. Mobarak HM et al (2014) The prospects of biolubricants as alternatives in automotive applications. Renew Sustain Energy Rev 33:34–43
2. Arumugam S, Sriram G (2012) Effect of bio-lubricant and biodiesel-contaminated lubricant on tribological behavior of cylinder liner-piston ring combination. Tribol Trans 55(4):438–445
3. Sadaka S, Boateng AA (2009) Pyrolysis and bio-oil. Cooperative Extension Service, University of Arkansas, US Department of Agriculture and county governments cooperating
4. Ting C-C, Chen C-C (2011) Viscosity and working efficiency analysis of soybean oil based bio-lubricants. Measurement 44(8):1337–1341
5. Mofijur M et al (2012) Prospects of biodiesel from Jatropha in Malaysia. Renew Sustain Energy Rev 16(7):5007–5020
6. Shahabuddin M et al (2013) Comparative tribological investigation of bio-lubricant formulated from a non-edible oil source (Jatropha oil). Ind Crops Prod 47:323–330
7. Cheenkachorn K, Fungtammasan B (2010) Development of engine oil using palm oil as a base stock for four-stroke engines. Energy 35(6):2552–2556
8. Syahrullail S et al (2011) Experimental evaluation of palm oil as lubricant in cold forward extrusion process. Int J Mech Sci 53(7):549555
9. Jayed MH et al (2009) Environmental aspects and challenges of oilseed produced biodiesel in Southeast Asia. Renew Sustain Energy Rev 13(9):24522462
10. Maleque MA, Masjuki HH, Haseeb ASMA (2000) Effect of mechanical factors on tribological properties of palm oil methyl ester blended lubricant. Wear 239(1):117–125
11. Jayadas NH, Prabhakaran Nair K, Ajithkumar G (2007) Tribological evaluation of coconut oil as an environment-friendly lubricant. Tribol Int 40(2):350–354
12. Kalam MA, Masjuki HH (2002) Biodiesel from palmoil—an analysis of its properties and potential. Biomass Bioenerg 23(6):471–479
13. Zeman A et al (1995) Biodegradable lubricants—studies on thermo-oxidation of metalworking and hydraulic fluids by differential scanning calorimetry (DSC). Thermochim Acta 268:9–15
14. Çakir M, Akçay IH (2014) Frictional behavior between piston ring and cylinder liner in engine condition with application of reciprocating test. Int J Mater Eng Technol 11(1):57
15. Cesur İ et al (2014) The effects of different fuels on wear between piston ring and cylinder. Adv Mech Eng 2014:1–8
16. Stachowiak GW, Batchelor AW, Stachowiak GB (2004) 2—Simulation of wear and friction. In: Gwidon AWB, Stachowiak W, Grazyna BS (ed) Tribology series, Elsevier, pp 13–23
17. Mehta DS, Masood SH, Song WQ (2004) Investigation of wear properties of magnesium and aluminum alloys for automotive applications. J Mater Process Technol 155–156:1526–1531
18. Holt JM (Tim), T.E.C.Y.H. (1996) Structural alloys handbook. CINDAS/Purdue University, West Lafayette, IN
19. Boyer HE, Gall TL (1985) Metals handbook. American Society for Metals, Materials Park, OH

20. Zulkifli NWM et al (2013) Wear prevention characteristics of a palm oil-based TMP (trimethylolpropane) ester as an engine lubricant. Energy 54:167–173
21. Lee EJ et al (2010) Morphology and toughness of abrasive particles and their effects on the friction and wear of friction materials: a case study with zircon and quartz. Tribol Lett 37 (3):637–644
22. Masjuki HH, Maleque MA (1996) The effect of palm oil diesel fuel contaminated lubricant on sliding wear of cast irons against mild steel. Wear 198(1–2):293299

Effect of Friction Stir Welding Parameters on the Peak Temperature and the Mechanical Properties of Aluminum Alloy 5083-O

Mostafa M. El-Sayed, Ahmed Y. Shash, Tamer S. Mahmoud and Mahmoud Abd Rabbou

Abstract In the present investigation, a 3D transient heat transfer model is developed to simulate the thermal distribution of aluminum alloy 5083-O friction stir welded by using Abaqus software. A 6 mm AA5083-O plates were friction stir welded at different conditions; two tools with tapered smooth and cylindrical threaded pin profiles, and 50, 100, 160 mm/min welding speeds at a constant rotational speed of 400 rpm. The temperature was measured using an infrared thermal image camera during the welding process at each operation condition. The measured temperature by IR camera was compared with temperatures obtained using the Abaqus. The welded joints were checked by visual inspection, macrostructure and microstructure evolution, in addition to tensile strength and hardness profiling. The welding speed and tool pin profile variations have a small effect on the peak temperature of the welded joints. The defect free welded joints were obtained at 50, 100, 160 mm/min welding speeds using a threaded tool pin profile. The tensile strength values obtained by using a threaded tool pin profile at all welding speeds are better than those obtained by using a tapered tool pin profile where the best one is at 50 mm/min welding speed. In terms of hardness results, the threaded tool pin profile gives better results at all welding speeds than the tapered tool pin profile.

Keywords Friction stir welding · Tool pin profile · Mechanical properties · Finite element modeling

M.M. El-Sayed · A.Y. Shash (✉) · T.S. Mahmoud · M.A. Rabbou
Mechanical Design and Production Engineering Dept, Cairo University, Giza 12311, Egypt
e-mail: ahmed.shash@cu.edu.eg

M.M. El-Sayed
e-mail: mostafamohammed30@yahoo.com

M.A. Rabbou
e-mail: mahmoud.abdrabou@gmail.com

A. Öchsner and H. Altenbach (eds.), *Improved Performance of Materials*, Advanced Structured Materials 72, DOI 10.1007/978-3-319-59590-0_2

1 Introduction

Friction Stir Welding (FSW) was invented by Wayne Thomas at TWI (The Welding Institute), in the UK in 1991. FSW is a solid state joining process, in which the objects are welded together without reaching the melting point of the base metal [1].

In FSW, a non-consumable shouldered tool with a profiled pin is rotated and immersed into the abutting faces of work-pieces, thereby generating frictional heating at tool-work piece interface, leading to softening of the work-piece material. After that, the tool is moved along the joint line producing a continuous welded joint [2].

FSW is considered to be environmentally friendly because there is no cover gas. Since no melting occurs during FSW, it can be used for joining the 2xxx and 7xxx aluminum alloys which are difficult to weld using traditional methods due to the poor solidification of the microstructure and porosity in the fusion zone. Also, it can be used for welding any kinds of materials, material composites, and dissimilar materials, with ease [3].

These days, FSW is applied in many industries such as: aerospace, shipbuilding and automotive industries [4].

There are many parameters affecting the mechanical properties and microstructure of friction stir welded joints. These parameters are: tool design, rotational speed, welding speed, axial force, plunge depth and tool tilt angle. Rotation speed affects the frictional heat, welding speed control which affects the heat generated, tool tilt angles which affects the efficiency of the weld, plunge depth which produces sound welds, axial force which generates further heating and tool design which affects the flow and the power required for the process [5].

The microstructure of aluminum friction stir welded joints is classified into four zones. This classification is based on the effect of the heat and plastic deformation on the material. These zones are: the first one is an unaffected zone in which neither heating nor plastic deformation affect the microstructure of the material. The second one is the heat affected zone (HAZ) which is adjacent to the unaffected zone, where the heat generated has no effect on the microstructure of the material. The third one is the thermo-mechanically affected zone (TMAZ) which is adjacent to the HAZ, where both heat and plastic deformation affect the microstructure but, there is no recrystallization occurred because the deformation strain is not enough. The fourth one is the dynamically recrystallized zone (DXZ) which is lying in the weld center line beside the TMAZ and subject to both higher deformation strain and higher temperature which cause recrystallization of the material resulting in finer grains sizes [6].

Many investigators [7–11] have studied and reported on the effect of FSW parameters on the mechanical properties and microstructure of friction stir welded aluminum joints.

FSW has three main phases: the plunge phase, dwell phase and welding phase [7]. The generated heat from the FSW process is frictional heat and plastic dissipation heat generation. The first one is due to the contact between the tool and work-piece, while the second one is due to plastic energy dissipation [12].

Since FSW has both thermal and mechanical loads, simulation of that process is quite complicated to obtain the thermal history and stresses produced from it. Some investigators have built a heat transfer model to predict the temperature distribution during the FSW process, while others have built a thermo-mechanical model to simulate the plunge phase during the process. However, a few investigators have built a heat and material flow models to simulate the flow of material during the process [13].

2 Experimental Investigations

2.1 Numerical Simulation

A **3D** transient heat transfer finite element model was developed to simulate the thermal distribution during friction stir welding of **AA5083-O** using the Abaqus software. The part dimensions are 100 × 50 × 6 mm for one piece where half of welding was simulated to reduce running time. The heat losses due to convection and radiation are neglected. Temperature dependent properties of the model are shown in Table 1.

Boundary conditions (**BCs**): the model is completely fixed in all directions except along the welding line, where it is partially fixed.

Load: a heat flux load is subjected to the surface of the part with a certain value. This value is obtained from the following formula:

$$\text{Heat flux}(\text{Q}) = \frac{heat\ input(q)}{Area(A)} \left(\text{W}/\text{m}^2\right)$$

Table 1 The temperature dependent properties of AA5083

Temperature	Conductivity (W/m °C)	Specific heat (J/kg °C)	Density (kg/m^3)
−20	112.5	924.1	2673.9
80	122.7	984.2	2642.7
180	131.6	1039.6	2629.4
280	142.3	1081.2	2611.5
380	152.5	1136.6	2589.3
480	159.5	1178.2	2567
580	177.2	1261.4	2549.2

Heat input (q) is calculated from the *Frigard* equation

$$q = \int_0^R 2\omega\pi\mu P r^2 dr \ (\mathrm{W}),$$

$$\omega = \frac{2\pi n}{60}$$

$$q = \int_0^R \frac{2}{30}\pi^2\mu P n r^2 dr = \frac{1}{45}\pi^2\mu P n (R^3 - r^3)$$

where

ω : Angular velocity (rad/sec)

n : Rotational speed(rpm) $\qquad P = \frac{F}{A}$

The following assumptions are considered:

Friction coefficient $(\mu) = 0.4$ $\qquad$ Axial force (F) = 2000 N

$A = \pi(R - r)^2\ \mathrm{mm}^2$

Shoulder radius (R) = 12.5 mm $\qquad$ Pin radius (r) = 4 mm

Since the friction coefficient, axial force, shoulder radius and pin radius are constants, changing the rotational speed values results in changed heat flux values leading to a change in the temperature distribution. Then, $\mathbf{Q = 2.5 \times 10^6\ W/m^2}$ (at **400 rpm**).

Figure 1 shows both boundary conditions and load subjected to the part.

Meshing: The element type is heat transfer DCC3D8 with 8-node convection/diffusion brick. Figure 2 shows the meshing of the part.

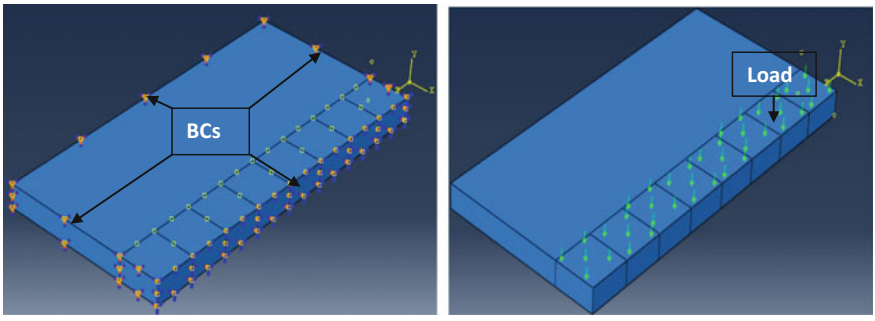

(a) BCs subjected to the part (b) Heat flux load subjected to the part

Fig. 1 BCs and load on the part

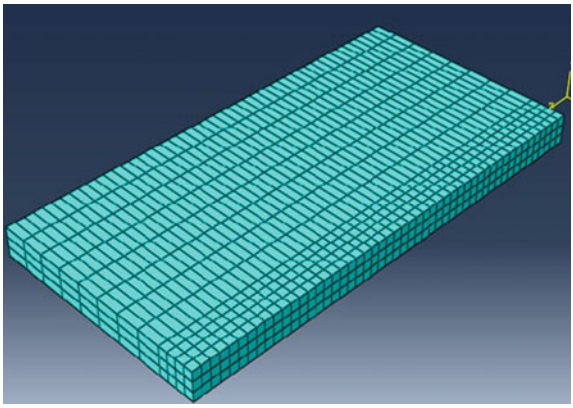

Fig. 2 Meshing of the part

2.2 Welding Process and Operation Conditions

The tool material is **K720** with **57 HRC**. Two tools with two different pin profiles, cylindrical threaded and tapered smooth pin profiles, were used. Figure 3 shows the schematic drawing of each tool. The wok piece material is **AA5083-O** with dimensions of 100 × 50 × 6 mm which is half of the welded joint. Tables 2 and 3 show the material chemical composition and mechanical properties respectively.

A universal milling machine was used to perform the friction stir welding process. The work piece was fixed on the machine by a mechanical vice as shown in Fig. 4. Table 4 shows the FSW parameters. **Fluke infra-red** thermal image camera shown in Fig. 5 was used to measure the temperature at each operation condition.

2.3 Material Characterization

A rectangular specimen was cut out from each friction stir welded joint perpendicular to the welding line. The samples were grinded using emery papers down to 2500 grade followed by polishing using 0.3 μm alumina suspension solution. The surfaces of the specimens were etched using Poulton's reagent [2 ml HF, 3 ml HCl, 20 ml HNO_3, 175 ml H_2O]. The microstructure examination was carried out using an OLYMPUS optical metallurgical microscope, equipped with a high resolution digital camera for the investigation of the microstructure.

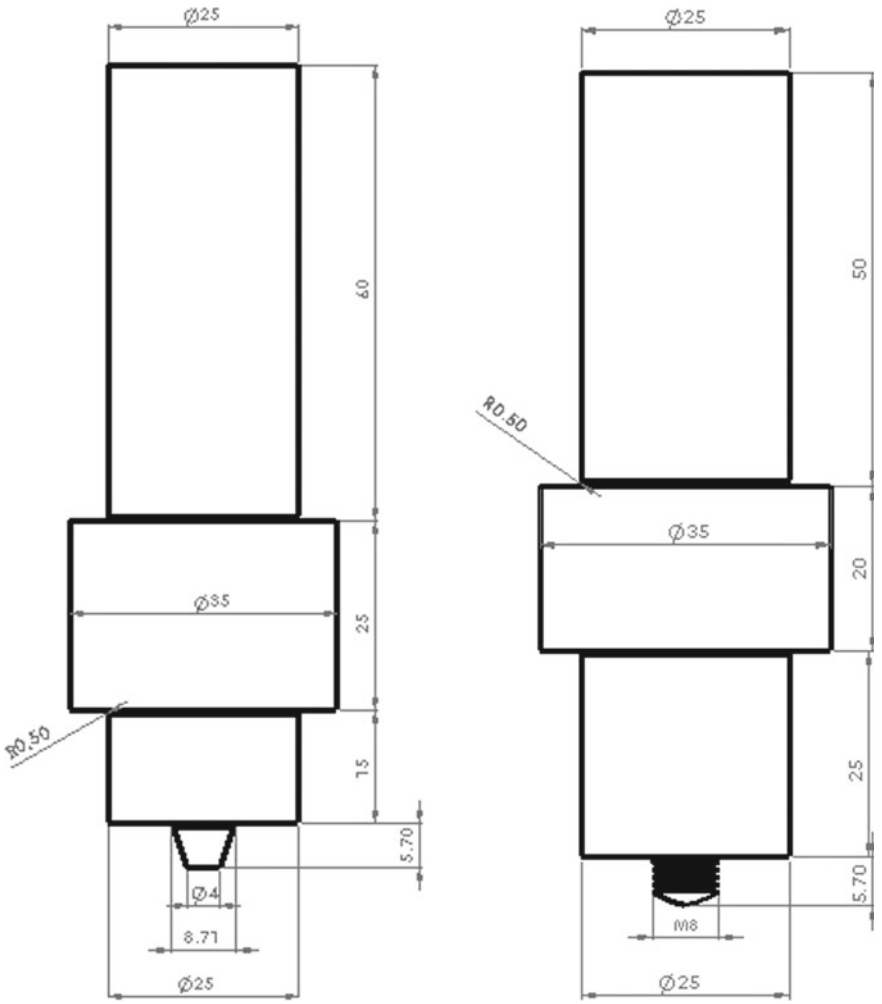

Fig. 3 Tools geometry

Table 2 The chemical composition of AA5083-O

Si	Fe	Cu	Mn	Mg	Zn	Ni	Pb	Sn	Al
0.1737	0.2867	<0.0010	0.4623	4.298	0.0075	<0.005	<0.002	<0.002	Balance

Table 3 The mechanical properties of AA5083-O

Ultimate tensile strength (σ_u)	Yield strength (σ_y)	Elongation (%)	Vickers Hardness (HV)
272	176	14	75

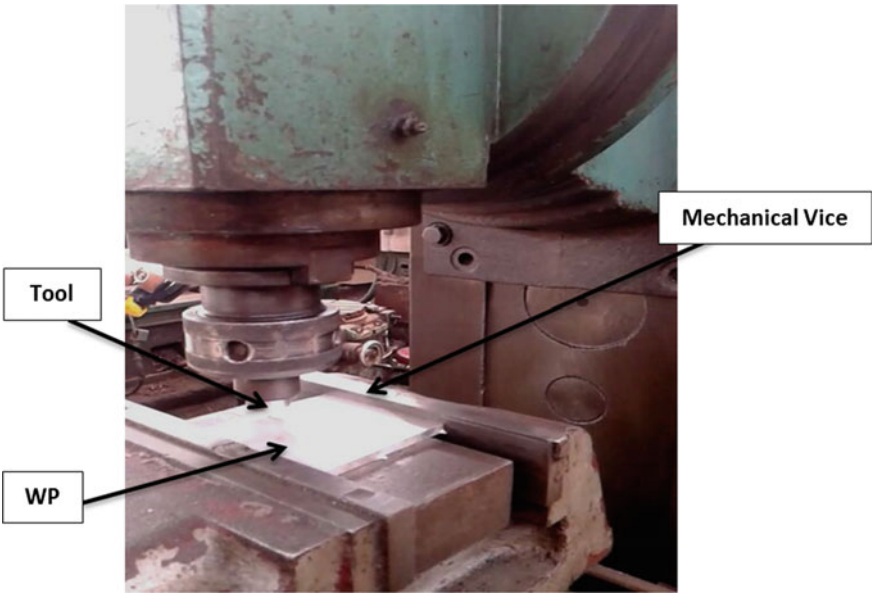

Fig. 4 Machine set-up

Table 4 FSW parameters

Process parameters	Tool pin profile	Welding speed (mm/min)	Rotational speed (rpm)	Plunge depth (mm)	Tool tilt angle (°)
Value	Cylindrical threaded and tapered smooth	50, 100 and 160	400	0.2	0

Fig. 5 Fluke IR thermal image camera

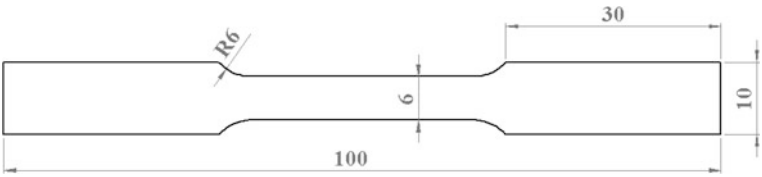

Fig. 6 Schematic drawing of tension test specimen (Thickness = 6 mm)

2.4 Mechanical Properties

The mechanical properties, mainly tensile strength and hardness, were measured for each sample.

2.4.1 Tensile Strength

Three tension test samples were taken from each welded joint and cut according to ASTM standard dimensions as shown in Fig. 6, tested on a universal testing machine and the average values were calculated for each case.

2.4.2 Microhardness Test

A rectangular specimen was cut out from each friction stir welded joint perpendicular to the welding line. The microhardness tests were conducted on a Zwick/Roell hardness testing machine.

3 Results and Discussions

3.1 Numerical Simulation and Temperature Distribution

After running the job of the model, the simulation is obtained and a path is taken along the line perpendicular to welding line to graph the temperature distribution. Figure 7a shows the temperature profile during simulation and Fig. 7b shows the temperature distribution curve obtained from simulation. It is observed that the peak temperature obtained from simulation in welding area is 448.8 °C and the temperature at 50 mm far from weld centre line is about 69.5 °C.

Figure 8 shows the variation of peak temperature at different welding speeds. It is observed from the graph that the highest peak temperature is at **50 mm/min** welding speed and the lowest one is at **150 mm/min** for the same tool pin profile. It is noticed that the tool pin profile does not strongly affect the peak temperature of the joints during welding process.

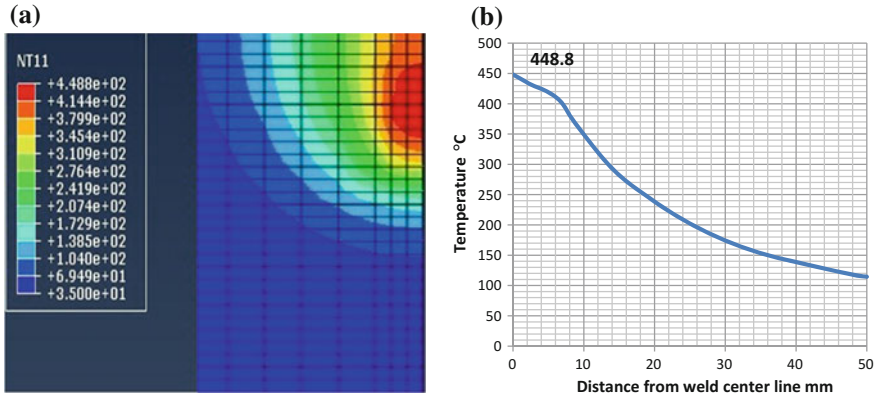

Fig. 7 **a** Temperature profile. **b** Simulated temperature distribution

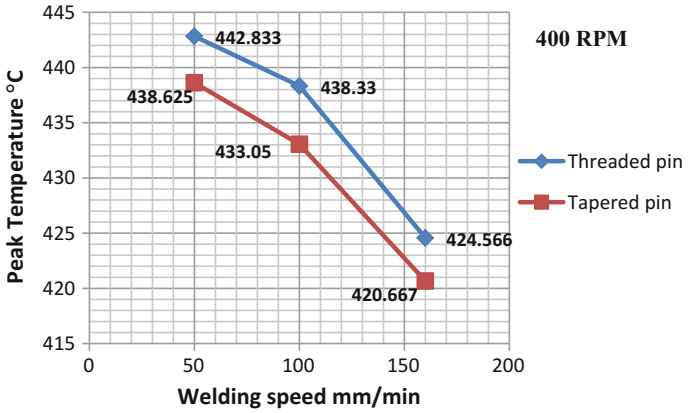

Fig. 8 Variation of peak temperature due to variation of welding speed and tool pin profile at 400 rpm

Figure 9 shows the comparison between the simulated temperature distribution obtained by the Abaqus software and the measured temperature distribution obtained by IR camera at **400 rpm** rotational speed and **50 mm/min** welding speed.

3.2 Surface Morphology

The upper surface macrographs of the welded joints at different welding conditions are shown in Fig. 10. It is observed from figure that the welded joints by threaded and tapered tool pin profile have an accepted surface appearance at all welding speeds where there are no grooves or surface-open tunnel defects.

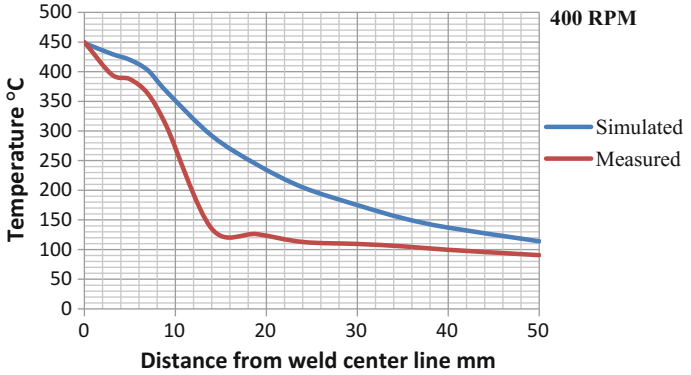

Fig. 9 Simulated and experimental temperature distribution

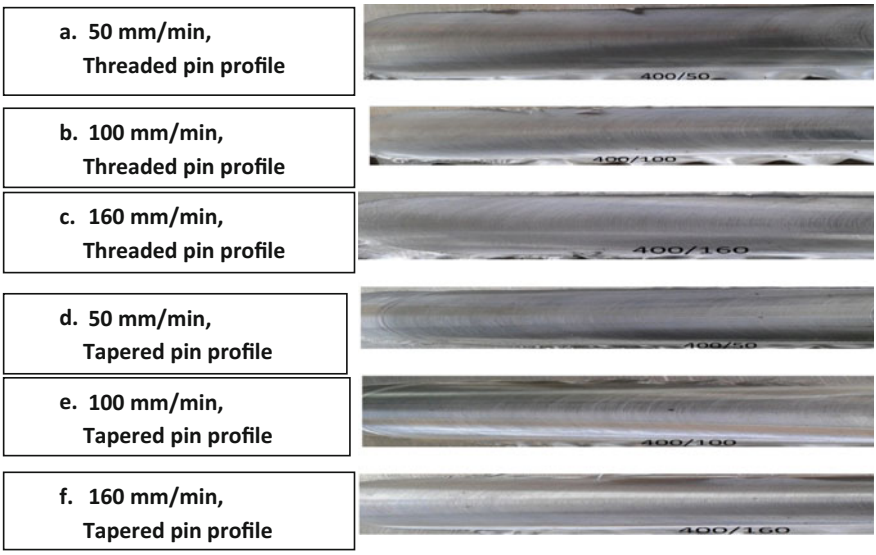

Fig. 10 Surface morphologies at different operating conditions

3.3 Macrostructure and Microstructure Evolutions

Figure 11 shows the macrostructure and microstructure observation for each sample. As observed from this figure, the defect free welds are obtained when welding process is performed using cylindrical threaded tool pin profile at all welding speeds values. While tunnel defects appeared when using smooth tapered pin